Available online at www.sciencedirect.com
SCIENCE DIRECT®
Journal of Solid State Chemistry 177 (2004) 3105–3113
JOURNAL OF SOLID STATE CHEMISTRY
http://elsevier.com/locate/jssc

Microdomain texture and microstructures of Fe^{4+}-containing $CaTi_{0.4}Fe_{0.6}O_{3-\delta}$

Jesús Canales-Vázquez,[a] Filipe M. Figueiredo,[b,c,*] João C. Waerenborgh,[d] Wuzong Zhou,[a] Jorge R. Frade,[b] and John T.S. Irvine[a]

[a] School of Chemistry, University of St. Andrews, St Andrews, Fife KY16 9ST, Scotland, UK
[b] Ceramics and Glass Engineering Department, CICECO, University of Aveiro, 3810-193 Aveiro, Portugal
[c] Science and Technology Department, U. Aberta, R. Escola Politécnica 147, 1269-001 Lisbon, Portugal
[d] Chemistry Department, Instituto Tecnológico e Nuclear, Estrada Nacional 10, 2686-953, Sacavém, Portugal

Received 23 January 2004; received in revised form 12 May 2004; accepted 13 May 2004

Available online 8 July 2004

Abstract

A study of the structure of Fe^{IV} $CaTi_{0.4}Fe_{0.6}O_{3-\delta}$ is presented and compared to data on the Fe^{III} counterparts. The powder XRD pattern was dominated by a simple cubic perovskite unit cell; however, some small peaks indicated an orthorhombic distortion. All peaks could be indexed using a space group analogous to the Fe^{III} phase $Ca_3TiFe_2O_8$. From HRTEM the strong cubic peaks are well explained by the superposition of three equivalent and mutually perpendicular orthorhombic unit cells. TEM analysis further revealed a microdomain structure consisting of disordered intergrowths of $CaTiO_3$- and $Ca_3TiFe_2O_8$-like phases. Mössbauer spectra show that ca. 4% of the Fe cations are in the 4+ oxidation state. Results suggest that the Fe^{4+} cations are associated with octahedral coordination and hence are associated with the $CaTiO_3$-like regions, transition regions between the $CaTiO_3$- and $Ca_3TiFe_2O_8$ intergrown phases and the domain boundaries. Structural models for the intergrowths are proposed based on HRTEM image simulations.

Keywords: Titanates; Structure; Microdomains; HRTEM; Image simulation; Mössbauer spectroscopy

1. Introduction

It is well known that partial substitution of Ti^{4+} by Fe^{3+} in $CaTiO_3$ leads to the formation of oxygen vacancies in order to maintain the electroneutrality in the crystal. Fe cations will thus originate a significant increase of both the ionic and hole–electronic conductivities. The material becomes a mixed oxygen ionic and electronic conductor with reasonable ambipolar conductivity [1–3] and, therefore, it has been studied as a membrane material for oxygen or hydrogen electrochemical permeation [1,4–6]. Part of the vacancies become ordered in FeO_4 tetrahedral chains while the other part remains disordered occupying pentacoordinated sites around Fe^{3+} [7–12]. The border between ordered and disordered phases is a function of the Fe substitution level, the temperature and the oxygen partial pressure. All these three factors determine the concentration of oxygen vacancies in the structure. Totally reduced materials, i.e., materials where all Fe appears as Fe^{3+}, have been widely studied since the late 1970s [7,8] and a phase diagram has been recently proposed [9]. According to this diagram, the order–disorder transition occurs at ca. 1150°C for $x = 0.50$ whereas for $x = 0.667$ it occurs at higher temperatures, x being the fraction of Fe. However, the presence of a small fraction of tetravalent iron may modify the structure. Indeed, published X-ray diffraction (XRD) patterns obtained with oxidized and reduced samples revealed large differences: the oxidized materials ($x = 0.30$–0.60) have an apparent cubic cell [1,2] while the totally reduced counterparts are clearly orthorhombic [7,9,11].

*Corresponding author. Ceramics and Glass Engineering Department, CICECO, University of Aveiro, 3810-193 Aveiro, Portugal. Fax: +351-234-425300.
E-mail address: framos@cv.ua.pt (F.M. Figueiredo).

0022-4596/$ - see front matter © 2004 Elsevier Inc. All rights reserved.
doi:10.1016/j.jssc.2004.05.029

A similar behavior was described in the $Ca_{1-x}La_xFeO_{3-\delta}$ system by Alario-Franco and co-workers [13–16]. These authors, based in detailed transmission electron microscopy studies, suggested that the apparent cubic symmetry was a consequence of a set of mutually perpendicular microdomains of brownmillerite or $Ca_2LaFe_3O_8$ orthorhombic phases. They have gone further by putting forward a structural model of the domain boundaries where the oxygen excess (or the Fe^{4+}) is preferentially accommodated thus determining the domain size; more Fe^{4+} smaller domains. However, these findings have not been confirmed for materials in the $CaTi_{1-x}Fe_xO_{3-\delta}$ system.

In the present work, oxidized $CaTi_{0.4}Fe_{0.6}O_{3-\delta}$ was synthesized and its structure was investigated by XRD and high-resolution transmission electron microscopy (HRTEM) upon which a structural model is presented. These results are complemented by Mössbauer spectroscopy data on the valence, hence oxygen stoichiometry, and coordination of iron cations.

2. Experimental

Specimens with nominal composition of $CaTi_{0.4}Fe_{0.6}O_{3-\delta}$ were obtained by a classical ceramic route using high-purity TiO_2 (Merck), $CaCO_3$ (Merck) and Fe_2O_3 (Riedel-de Haën). The starting oxides were suspended in alcohol and mixed in Nylon® containers with zirconia balls for 2 h. The dried mixture was then calcined at 1100°C for 10 h at a temperature rate of 4 K/min and ball-milled again after cooling at room temperature. The resulting powder was sieved (30 μm mesh) and uniaxially pressed at 200 MPa into disks of ca. 10 mm in diameter. These disks were sintered in air at 1350°C for 2 h with heating/cooling rates of 5 K/min. The resulting ceramics were crushed in a mortar for the subsequent analyses.

Powder XRD patterns of the specimens were collected at room temperature using a Rigaku spectrometer with Cu$K\alpha$ radiation, scan ring speed of 0.05°/min and step width of 0.02°.

HRTEM images and selected area electron diffraction (SAED) were performed on a JEOL JEM 2011 electron microscope operating at 200 kV, equipped with a side-entry ±20° double tilt sample holder. The chemical homogeneity of the powders was assessed by energy dispersive X-ray spectroscopy (EDS) using an Oxford Link ISIS system. The samples were prepared by depositing a drop of an acetone suspension of $CaTi_{0.4}Fe_{0.6}O_{3-\delta}$ onto a perforated carbon-coated Cu grid. Simulations of the HRTEM images were carried out with the commercial software MacTempas PC version 1.7.9.

Mössbauer data recently obtained by the authors and reported in Ref. [12] were reevaluated in the present study considering distributions of quadrupole splittings, in light of the observed HRTEM domains structures. The same non-linear least-squares computer method was used [17]. The spectra were taken in transmission mode using a conventional constant-acceleration spectrometer (Wissel Instruments) and a 25 mCi ^{57}Co source in an Rh matrix. The velocity scale was calibrated at room temperature using an α-Fe foil. Isomer shifts are given relative to α-Fe at room temperature. The spectrum collected with the sample at 5 K was obtained using a liquid helium flow cryostat with temperature stability of 0.5 K.

3. Results and discussion

3.1. X-ray diffraction

Fig. 1 shows the powder XRD pattern of $CaTi_{0.4}Fe_{0.6}O_{3-\delta}$. The pattern is clearly dominated by a set of diffraction maxima (bottom line) characteristic of a simple cubic cell with the lattice parameter $a_p = 3.84(7)$ Å. However, a more detailed examination of the spectrum highlighted the presence of additional peaks, e.g., at $2\theta = 16.7°$, 27.5°, 35.4°, 37.1°, 44.5° with very low intensity, which along with the main peaks may be indexed onto an orthorhombic unit cell (space group $Pcm2_1$) with lattice parameters similar to those of $Ca_3TiFe_2O_8$ (Table 1).

The present result confirms previous observations by Iwahara and co-workers [1] who have reported a similar apparently cubic pattern for $CaTi_{1-x}Fe_xO_{3-\delta}$ ($x = 0.30$,

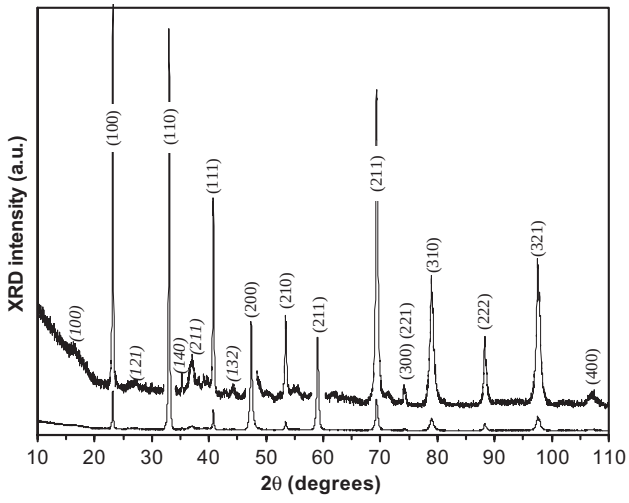

Fig. 1. Powder XRD pattern of $CaTi_{0.4}Fe_{0.6}O_{3-\delta}$ taken at room temperature. The main reflections are indexed on to a cubic unit cell (space group $Pm3m$). For clarity, the original pattern (bottom line) was multiplied by a factor of 10 and plotted on top. The additional reflections (in italic) are indexed to an orthorhombic unit cell (space group $Pcm2_1$), possibly corresponding to $Ca_3TiFe_2O_8$.

Table 1
Structural parameters of $CaTi_{1-x}Fe_xO_{3-\delta}$

x	Space group	a (Å)	b (Å)	c (Å)	Ref.
0	*Pnma*	5.4424(1)	7.6417(2)	5.3807(1)	[18]
0.50	*Pnma*	5.437(1)	30.22(1)	5.489(1)	[21]
0.67	$Pcm2_1$	5.5295(3)	11.2045(6)	5.4379(3)	[19]
1.00	*Pcmn*	5.559(1)	14.771(2)	5.429(1)	[20]

0.50 and 0.60) prepared by a ceramic route in air. On the contrary, patterns of the reduced materials in the compositional range $0.50 \leqslant x \leqslant 1.00$ were indexed with orthorhombic unit cells formed as the result of the long range ordering of oxygen vacancies along the *b*-axis [7,11]. In these phases, the vacancies are ordered into planes containing tetrahedral Fe^{3+} which alternate with planes containing octahedrally coordinated Ti^{4+} and Fe^{3+}. These stacking sequences are formed in the (0*k*0) planes of the original orthorhombic perovskite cell, i.e., $CaTiO_3$ (space group *Pnma*, $a = 5.378$ Å, $b = 7.637$ Å, $c = 5.440$ Å). The number of tetrahedral layers increases with reducing oxygen substoichiometry, and thus with increasing Fe^{3+} concentration. Particularly stable motives appear for $Ca_2Fe_2O_5$ ($x = 1.00$), $Ca_3TiFe_2O_8$ ($x = 0.67$) and $Ca_4Ti_2Fe_2O_{11}$ ($x = 0.50$) that correspond to the ordered sequences of tetrahedra (T) and octahedra (O), OT, OOT and OOOT, respectively. The structural parameters of each one of these phases are given in Table 1. Disordered intergrowth of the mentioned phases occurs for intermediate values of x.

The likely presence of $Ca_2Fe_2O_5$, $Ca_3TiFe_2O_8$, $Ca_4Ti_2Fe_2O_{11}$, or a Fe-containing $CaTiO_3$-based perovskite should thus be considered in the indexing of the XRD patterns. Further TEM studies were required to study the presence of such phases.

3.2. Transmission electron microscopy

HRTEM studies reveal that $CaTi_{0.4}Fe_{0.6}O_{3-\delta}$ is not homogeneous on the nanometer scale. The SAED pattern shown in the inset of Fig. 2 reveals *d*-spacings of 11.2 Å along one of the axes, confirming that a simple cubic unit cell is not sufficient to describe the real structure of this material. This and all the remaining SAED patterns are indexed according to the $CaTiO_3$ $\sqrt{2}a_p \times 2a_p \times \sqrt{2}a_p$ (a_p is the unit cell parameter of a perovskite) orthorhombic unit cell, and the corresponding zone axis is noted with a subscripted "O". The stoichiometric similarity and the apparent *b*-axis being $3 \times a_p$ suggest that the unit cell should be similar to that of $Ca_3TiFe_2O_8$ [7], i.e., $\sqrt{2}a_p \times 3a_p \times \sqrt{2}a_p$ orthorhombic unit cell, space group $Pcm2_1$ with the cell dimensions $a = 5.53$ Å, $b = 11.2$ Å and $c = 5.44$ Å; this result is in agreement with the low intensity reflections on the XRD pattern (Fig. 1). In addition diffuse scattering along the

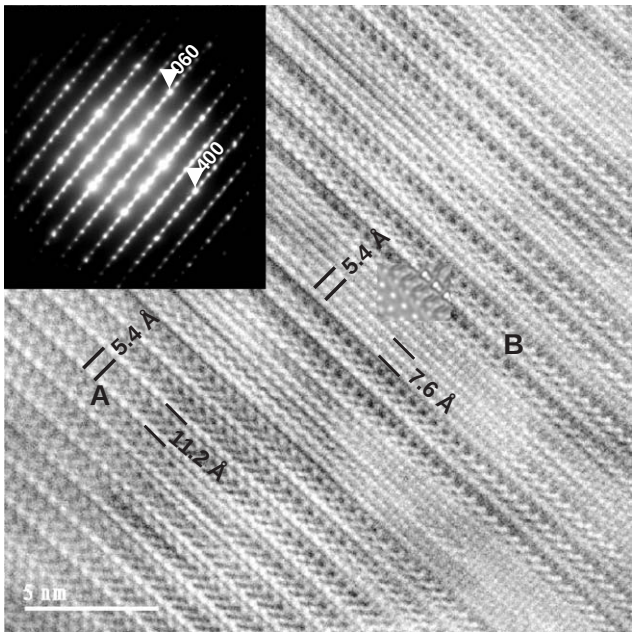

Fig. 2. HRTEM showing the intergrowths of two phases: (A) $Ca_3TiFe_2O_8$ and (B) $CaTiO_3$ viewed down the $[100]_O$ zone axis. The insets show the corresponding SAED pattern and a simulated image (defocus −400 Å, thickness 50 nm) of the intergrowths based on the model described in the text.

b^*-axis is clearly observed indicating a disorder phenomenon along that particular direction. Indeed, the corresponding HRTEM (Fig. 2) showed a complex irregular intergrowth of two phases, marked as A and B. The former is $Ca_3TiFe_2O_8$-like since its *b*-axis is measured to be 11.2 Å and the other principal axis is about 5.4 Å.The latter could be considered as $CaTiO_3$-like unit cell, i.e., $\sqrt{2}a_p \times 2a_p \times \sqrt{2}a_p$, as the corresponding *d*-spacings (7.8 and 5.5 Å) suggest. Occasionally some domains showing a longer *b*-axis of 15.5 Å were discernible, which would correspond to a $\sqrt{2}a_p \times 4a_p \times \sqrt{2}a_p$ unit cell (Fig. 3). Hence phases with different oxygen vacancy content or, in other words, different stacking sequences cohabit in "$CaTi_{0.4}Fe_{0.6}O_{3-\delta}$".

The relatively poor quality of the micrograph shown in Fig. 3 puts into evidence a certain instability of the sample under the beam. This may be related to the in situ reduction of the material resulting from a localized temperature increase at the beam incidence area paired to the reducing atmosphere inside the microscope chamber. Similar difficulties have been found during the study of other titanates. The instability of the material may also result from the partial reduction of Fe^{4+} [3,12].

Investigations carried out on some other crystals revealed predominant $Ca_3TiFe_2O_8$ domains as depicted with a HRTEM image and the corresponding SAED pattern in Fig. 4, showing a view on the $[101]_O$ projection. On the other hand, there existed some

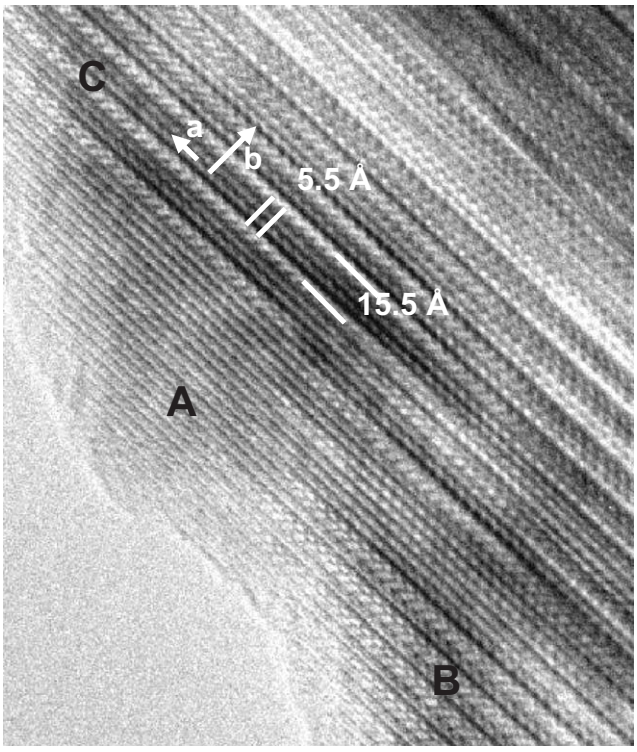

Fig. 3. HRTEM image showing the irregular intergrowths of (A) $Ca_3TiFe_2O_8$, (B) $CaTiO_3$ and (C) $Ca_4Ti_2Fe_2O_{11}$ (d-spacing 15.2 Å) viewed down the $[001]_O$ zone axis.

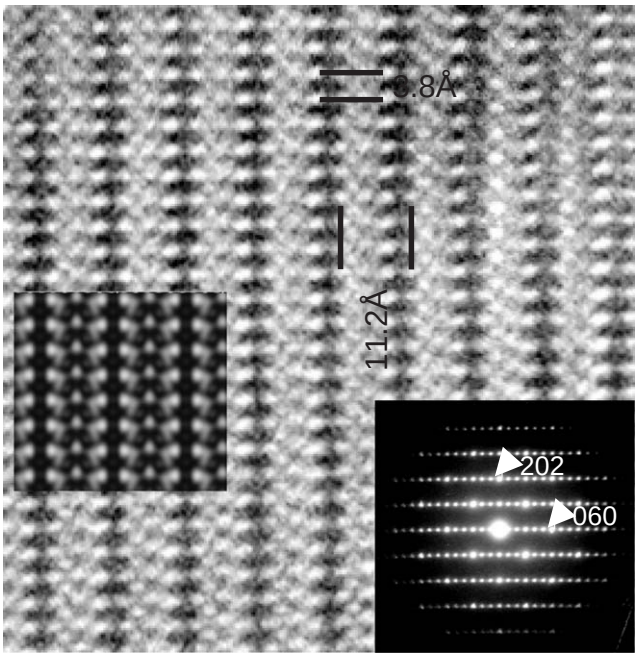

Fig. 4. HRTEM image and corresponding SAED pattern of a $Ca_3TiFe_2O_8$-like domain along the $[101]_O$ zone axis. The simulated image was taken at defocus −500 Å and thickness 101 nm.

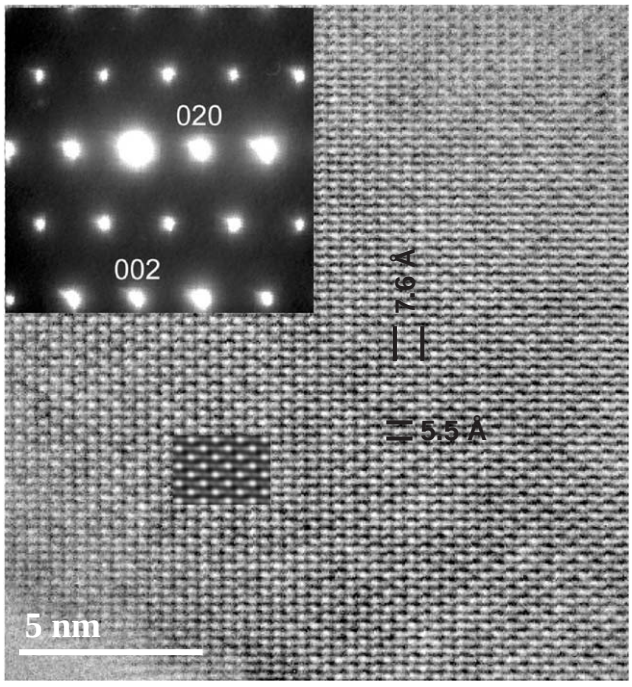

Fig. 5. HRTEM image showing a view down the $[100]_O$ zone axis on Fe doped $CaTiO_{3-\delta}$. The two insets show the corresponding SAED pattern and the simulated image (defocus −400 Å, thickness 50 nm), respectively. A model with 20% Fe substitution of the Ti sites in nano-ordered manner was used (see Table 2).

domains that correspond to the $CaTiO_3$ type structure as can be observed in Fig. 5, although in lower concentration. It is worth noting that the corresponding SAED patterns can obviously be indexed with the $CaTiO_3$ unit cell. However, simulation of the images allowed uncovering the presence of some Fe substituting Ti. Indeed, the diamond-shape contrast observed in the experimental image is not reproduced if the *B*-sites are exclusively occupied by Ti. The best result (inset of Fig. 5) was achieved when replacing Ti by Fe in 40% of two of the four available *B*-site positions. The atomic positions of the Fe-doped $CaTiO_3$ unit cell, listed in Table 2, were obtained by a simple transformation of the unit cell consisting on the replacement of Ti by Fe. The distances were kept the same since it was found that a variation of 0.1 Å had no apparent effect on the final result.

According to Grenier et al. [7,8], $Ca_3TiFe_2O_8$ is the $n = 3$ member of a series of intermediate phases $Ca_n(Ti,Fe)_nO_{3n-1}$ between the perovskite $CaTiO_3$ ($n = \infty$) and the brownmillerite $Ca_2Fe_2O_5$ ($n = 2$). As mentioned before, perovskite-like octahedra (O) layers "intergrow" with tetrahedra (T) layers forming ordered sequences. The brownmillerite shows a stacking sequence of one tetrahedron out of two, being consecutive tetrahedra layers orientated in opposite directions, i.e., following a sequence like …OTOT′ OTOT′…, along the *b*-axis, which implies that the *b*-axis is $4a_p$. Thus $Ca_3TiFe_2O_8$ is formed by inserting one tetrahedra layer into every three, i.e., …OOTOOT…. The exact stoichiometry of $n = 3$ phase $Ca_3TiFe_2O_8$ corresponds

Table 2
Atomic positions for the model $CaTiO_3$-like phase (space group *Pnma* and lattice parameters $a = 5.44$ Å, $b = 7.64$ Å and $c = 5.38$ Å) used in HRTEM image simulation in Fig. 5

Element	*x*-coordinate	*y*-coordinate	*z*-coordinate	Occupancy factor
Ca	0.00000	0.25000	0.01667	1.00000
Ca	0.50000	0.75000	0.51667	1.00000
Ca	0.00000	0.75000	0.98333	1.00000
Ca	0.50000	0.25000	0.48333	1.00000
Ti	0.00000	0.00000	0.50000	0.60000
Ti	0.00000	0.50000	0.50000	1.00000
Ti	0.50000	0.50000	0.00000	0.60000
Ti	0.50000	0.00000	0.00000	1.00000
Fe	0.00000	0.00000	0.50000	0.40000
Fe	0.50000	0.50000	0.00000	0.40000
O	0.21062	0.95991	0.69931	1.00000
O	0.26438	0.04009	0.22431	1.00000
O	0.73562	0.95991	0.77569	1.00000
O	0.78438	0.04009	0.30069	1.00000
O	0.92172	0.23750	0.49639	1.00000
O	0.07828	0.76250	0.50361	1.00000
O	0.76438	0.45991	0.27569	1.00000
O	0.71061	0.54009	0.80069	1.00000
O	0.23562	0.54009	0.72431	1.00000
O	0.28938	0.45991	0.19931	1.00000
O	0.42172	0.23750	0.00361	1.00000
O	0.57828	0.76250	0.99639	1.00000

Note that the Fe occupies only 40% of two of the four available *B*-site positions.

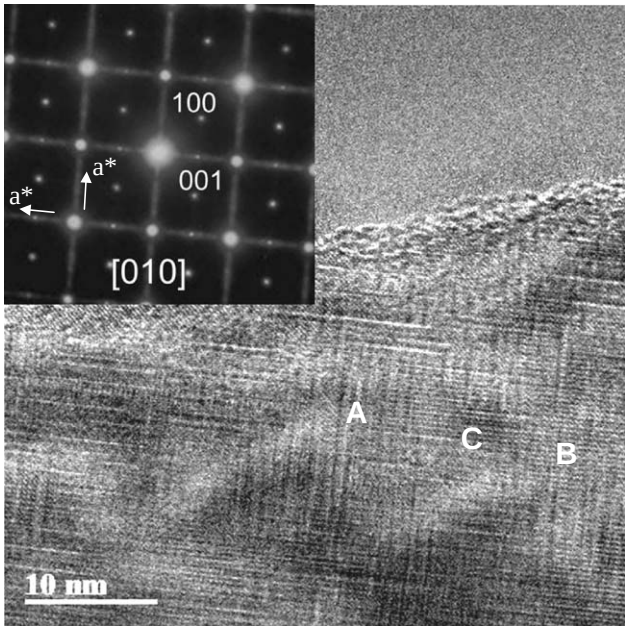

Fig. 6. HRTEM and SAED pattern showing the cubic symmetry of two sets of perpendicular domains consisting of (A) $Ca_3TiFe_2O_8$, (B) $CaTiO_3$ or (C) $Ca_3TiFe_2O_8/CaTiO_3$ intergrowths, viewed down the $CaTiO_3$ unit cell $[010]_O$ direction.

to lower Ti/Fe ratio in comparison with the composition prepared in the present work, thus one would also expect the presence of additional phase(s) with higher Ti/Fe ratio such as the $n = 4$ $Ca_4Ti_2Fe_2O_{11}$ if thermodynamic equilibrium was attained, at least if all Fe^{III} is assumed. Indeed, although quite rarely, a fringe spacing of about 15.5 Å characteristic of $Ca_4Ti_2Fe_2O_{11}$ [21] could also be observed (Fig. 3). It might, therefore seem surprising to see the formation of a Fe containing $CaTiO_3$-like phase in addition to the main phase $Ca_3TiFe_2O_8$, in "$CaTi_{0.4}Fe_{0.6}O_3$"; however, this largely reflects a significant degree of disorder, as the $n = 4$, and higher member phases, are particularly difficult to prepare due to the need for extensive long range ordering to take place. Such phases have been previously reported in the absence of excess oxygen [7,8]; however, the small amount of excess oxygen present in this system may also contribute to stabilising the cubic phase.

The pseudocubic symmetry suggested by the stronger reflections suggests that the above mentioned microdomains are aligned along three perpendicular directions in a manner that the symmetry of each set of microdomains is metrically cubic. Fig. 6 illustrates this situation where the principal diffraction reflections could be indexed considering either $Ca_3TiFe_2O_8$ or $CaTiO_3$ unit cells on the [010] projections. This could be interpreted as the result of the superposition of two patterns corresponding to two microdomains aligned in two perpendicular directions. The image in Fig. 6 further shows that these domains, smaller than 10 nm, consist mainly of $Ca_3TiFe_2O_8$, the majority phase in the compound, but also of $CaTiO_3$ or of intergrowths of the two phases. The existence of diffuse scattering is evidence of significant disorder in the planes perpendicular to the three axes that results from $CaTiO_3$ and $Ca_3TiFe_2O_8$ intergrowths. Not surprisingly, given the structural similarities, the present case has a strong resemblance to that reported for the oxidation of $Ca_2LaFe_3O_8$ to $Ca_2LaFe_3O_{8.235}$ when three sets of perpendicular microdomains, with the structure of the reduced stoichiometric $Ca_2LaFe_3O_8$ phase, were observed in the oxidized samples [13]. Like in $CaTi_{0.4}Fe_{0.6}O_{2.71}$, the size of the domains in $Ca_2LaFe_3O_{8.235}$ was approximately 10 nm and the powder XRD pattern of these latter samples could also be indexed in a cubic-symmetric unit cell with a lattice parameter of approximately 0.3848(3) Å [13]. Contrary to the calcium lanthanum ferrite composition, the structure in the bulk of the Ti-containing materials is very inhomogeneous, probably because the extent of the excess oxygen is much smaller in this case with overall stoichiometry as determined by coulometry [3] of $CaTi_{0.4}Fe_{0.6}O_{2.71}$ and consistent with Mössbauer spectroscopic data presented later. Therefore, the excess of oxygen, or the Fe^{4+} cations, may also be located at the border regions between different $Ca_3TiFe_2O_8$ domains. Consequently, changes in the oxygen stoichiometry

should be reflected not only in the size, as suggested for $Ca_2LaFe_3O_{8.235}$ [13,16], but also in the level of structural inhomogeneity in the bulk of the domains. Moreover, the microdomain textured $Ca_{0.63}La_{0.37}FeO_{3-\delta}$ phase was obtained after quenching from high temperature (1400°C) in air, while the $CaTi_{0.4}Fe_{0.6}O_{2.71}$ specimen forms during a slow cooling process [13]. One further difference between these iron based phases and the Fe, Ti phases is clearly the presence of Ti^{4+}, which facilitates the occurrence of perovskite-like domains, possibly also including some of the Fe^{4+}.

To date, it has not been well established how different phases are connected along the *b*-axis; connection via oxygen planes seems the most intuitive approach. For the $CaTiO_3$ phase the choice is quite easy since the oxygen planes are somewhat equivalent. However in $Ca_3TiFe_2O_8$, there exist several possibilities arising from the …OOTOOT… stacking sequence. One might think that because $CaTiO_3$ is made uniquely from BO_6 octahedra, the most likely oxygen plane to form the interface with $Ca_3TiFe_2O_8$ would be one linking two consecutive octahedra in the stacking sequence. Oxygen planes where tetrahedral co-ordination is involved would be chemically different, although the connection is possible as it occurs for $Ca_3TiFe_2O_8$ or the brownmillerite $Ca_2Fe_2O_5$. Therefore, a model of intergrowth was built by joining the two separated unit cells on an oxygen plane as marked in Fig. 7c and then the images were calculated for the operating conditions. As it can be observed in the inset of Fig. 2, the fitting is satisfactory in this case. Other possibilities, including O–T connection, were also attempted leading to simulated images that did not correspond to the experimental one.

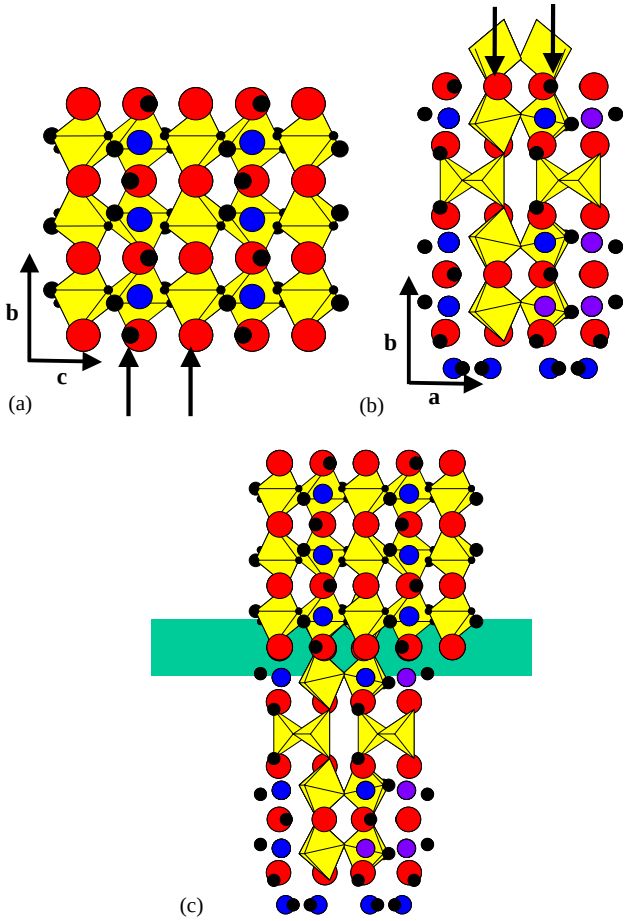

Fig. 7. Schematic representation of $CaTiO_3$ (a), $Ca_3TiFe_2O_8$ (b) and the intergrowth of the two phases (c). Arrows mark the oxygen planes that define the interface.

3.3. Mössbauer spectroscopy

The in situ high temperature powder XRD and Mössbauer spectroscopy analyses has shown that X-ray diffractograms [24] and Mössbauer spectra [12] of the $CaTi_{0.4}Fe_{0.6}O_{3-\delta}$ sample annealed at 1000°C do not change in the temperature range 290–900°C and are identical within experimental error to those obtained for the present $CaTi_{0.4}Fe_{0.6}O_{3-\delta}$ sample annealed at 1350°C. These results suggest that the microstructures of both Fe^{4+}-containing $CaTi_{0.4}Fe_{0.6}O_{3-\delta}$ samples are very similar and that it is reasonable to discuss and compare the Mössbauer data of the 1000°C annealed sample with the microdomain texture of the present 1350°C annealed sample, both cooled down in the same conditions.

The analysis of the Mössbauer spectra of $CaTi_{0.4}Fe_{0.6}O_{3-\delta}$ (Fig. 8) showed that, besides a small amount of Fe^{4+}, only two different coordinations for Fe^{3+} (4 and 6) are detected [12]. The absence of 5-coordinated Fe^{3+} (CN5-Fe^{3+}), detected in most $CaTi_{1-x}Fe_xO_{3-\delta}$ perovskites with lower Fe content, is consistent with the ordering of the anion vacancies observed with TEM in $CaTi_{0.4}Fe_{0.6}O_{3-\delta}$. Furthermore, the fraction of Fe^{4+} estimated from the Mössbauer spectra (4%) is in excellent agreement with estimates based on independent oxygen stoichiometry measurements [3].

At room temperature, the contribution of 6-coordinated Fe^{3+} (CN6-Fe^{3+}) consisted of two broad peaks. Two quadrupole doublets had to be considered in order to obtain a reasonable fit of this contribution [12]. The estimated hyperfine parameters for these doublets were consistent with Fe^{3+} in octahedral coordination. However the fact that the corresponding contribution had to be approximately described by two quadrupole doublets revealed that there is a large number of different nearest-neighbour cation arrangements around CN6-Fe^{3+} as explained in Ref. [12]. The microdomain texture and the disordered $CaTiO_3$–$Ca_3TiFe_2O_8$ intergrowths in the bulk of the domains observed by TEM supports this hypothesis and suggest the reanalysis of the $CaTi_{0.4}Fe_{0.6}O_{3-\delta}$ spectrum.

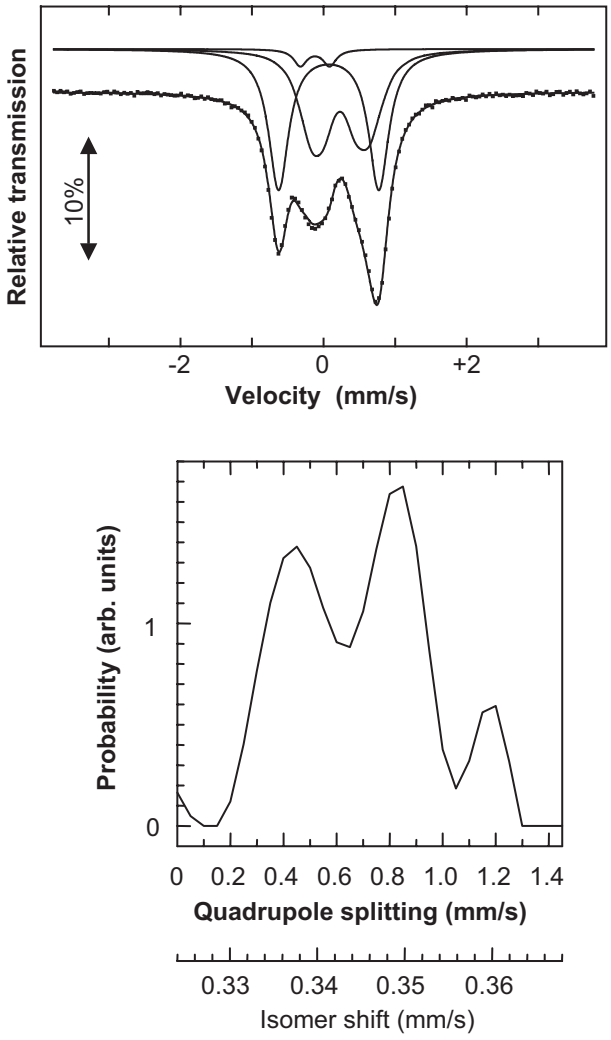

Fig. 8. Mössbauer spectrum of $CaTi_{0.4}Fe_{0.6}O_{3-\delta}$ taken at room temperature. The calculated function plotted on the experimental points is the sum of two doublets due to Fe^{4+} and CN4-Fe^{3+}, and a distribution of quadrupole splittings and isomer shifts assigned to CN6-Fe^{3+}. This distribution is represented at the bottom of the figure.

The 4-coordinated (CN4-Fe^{3+}) and the Fe^{4+} contributions were fitted in the same way considering two quadrupole doublets of lorentzian lines. The CN6-Fe^{3+} contribution was, however, approximated by a distribution of quadrupole splittings (QS). The best fit was obtained if a slight increase in the isomer shift, IS, of only ≈ 0.03 mm/s for each mm/s increase in QS, was considered. No strong dependence of IS on QS is therefore observed, confirming the absence of CN5-Fe^{3+}. Three maxima are observed in the final QS distribution (Fig. 8). The most intense ones correspond to average values $\langle IS \rangle \approx 0.34$ mm/s, $\langle QS \rangle \approx 0.43$ mm/s and $\langle IS \rangle \approx 0.35$ mm/s, $\langle QS \rangle \approx 0.83$ mm/s, similar to the hyperfine parameters estimated for the two quadrupole doublets attributed to CN6-Fe^{3+} in the former fit [12]. A third minor maximum is detected by the QS distribution approach with $\langle IS \rangle \approx 0.36$ mm/s, $\langle QS \rangle \approx 1.2$ mm/s.

QS values of CN6-Fe^{3+} in the $CaTiO_3$-type phase should be similar to those observed in low Fe^{3+}-containing $CaTi_{0.95}Fe_{0.05}O_{3-\delta}$ perovskites, that is, in the range 0.21–0.25 mm/s [12]. However, the concentration of Fe in the $CaTiO_3$-type phase may well be much lower than in the predominant $Ca_3TiFe_2O_8$, which accounts for 90% of the total number of formula units. Therefore, it is not surprising that the probability of QS values in the range 0.20–0.25 mm/s is very low in Ca $Ti_{0.4}Fe_{0.6}O_{3-\delta}$ (Fig. 8).

As referred to above, the $Ca_3TiFe_2O_8$ structure may be conveniently described as regular sequences …TOO TOOTOO… of tetrahedrally and octahedrally coordinated transition metal layers. The QS value of the CN6-Fe^{3+} distribution of quadrupole splittings obtained for $CaTi_{0.4}Fe_{0.6}O_{3-\delta}$ is 0.83 mm/s, slightly larger than $QS \approx 0.73$ mm/s reported for CN6-Fe^{3+} in the ordered …TOOTOOTOO… structure of $Ca_3TiFe_2O_8$ [10]. The larger QS values, as well as the intermediate QS values, in the range 0.20–0.80 mm/s in $CaTi_{0.4}Fe_{0.6}O_{3-\delta}$ may reflect the presence of Fe^{3+} with Fe^{4+} as next-nearest neighbours in the domain boundaries [14,16] and in the border regions between $CaTiO_3$- and $Ca_3TiFe_2O_8$-type phases. In such interfaces the tetrahedral layers are interrupted giving rise to …OOTOOTOOOOOOO…. These sites would then be preferential sites for the stabilization of Fe^{4+} cations. The reduction to CN4-Fe^{3+} ions is expected to occur as a result of a $Fe^{4+} \rightleftharpoons$CN4-$Fe^{3+}$ transition occurring via pentacoordinated Fe^{3+} intermediates, as previously suggested on the basis of measurements of oxygen stoichiometry changes by a solid electrolyte potentiometric–coulometric technique [3]. Due to the small size of the different domains and the high level of inhomogeneity inside them, these border regions should represent a significant fraction of the total sample.

According to the estimated relative area "*I*" (Table 3) the relative fractions of CN4-Fe^{3+} and CN6-Fe^{3+} are similar. This result is consistent with the …TOOTOO-TOO… structure of $Ca_3TiFe_2O_8$ where the number of the O-layers is twice that of the T-layers, and all Ti cations are octahedrally coordinated, as already suggested for the totally reduced materials [10,11]. Consequently, the number of octahedral sites available for Fe^{3+} will be approximately equal to the number of tetrahedral sites, in agreement with area *I* estimations. Note that the proportion of total Fe cations in the $CaTiO_3$ phase, as indicated from HRTEM image simulations (see Fig. 5 and related explanation) should be rather small because this phase only accounts for less than about 10% of the total number of formula units.

The analysis of the 5 K spectrum could be performed assuming only one magnetic sextet for CN6-Fe^{3+} but with significantly large peak widths $\Gamma \approx 0.7-0.9$ mm/s

Table 3
Parameters estimated from the Mössbauer spectra taken at 293 and 5 K of $CaFe_{0.6}Ti_{0.4}O_{3-\delta}$

	293 K				5 K				
	IS	QS	Γ	I	IS	ε	B_{hf}	Γ	I
CN4-Fe^{3+}	(0.34)	(0.43)							
CN6-Fe^{3+}	(0.35)	(0.83)	0.25	46%	0.47	−0.25	49.6	0.70	46%
	(0.36)	(1.18)							
Fe^{4+}	−0.01	0.43	0.22	4%	0.07	−0.27	34.0	0.34	4%

IS isomer shift relative to metallic α-Fe at 293 K, QS quadrupole splitting, B_{hf} magnetic hyperfine field, ε quadrupole shift, Γ peak width and I relative area. Values between brackets represent the average IS and QS of the local maxima in the QS distribution fitted to the 293 K spectrum.

(Table 3). The broadness of the peaks reveals the large number of different next-nearest-neighbor configurations around CN6-Fe^{3+}. The estimated I at 5 K and room temperature are the same within experimental error as already observed for the totally reduced materials [10]. The differences observed between the IS and magnetic hyperfine field values estimated for CN4-Fe^{3+} and CN6-Fe^{3+} agree with those observed in brownmillerite at 5 K [22,23]. The estimated magnetic hyperfine field values are however lower in $CaTi_{0.4}Fe_{0.6}O_{3-ä}$ probably due to the lower Fe concentration.

4. Conclusions

The structure of Fe^{4+}-containing perovskite-based oxides ($CaTi_{1-x}Fe_xO_3$) may be very different from that observed in the same material prepared under reducing conditions. In such cases, the first apparent difference is often found in routine powder XRD analysis. The pattern of the oxidized samples corresponds to that of a pseudocubic unit cell whilst lower symmetry is more evident for the totally reduced compounds. In a superficial analysis, the differences are simply interpreted as an increase in symmetry for the oxidized samples. However, TEM reveals a far more complex structure characterized by a microdomain texture where the domains are aligned perpendicularly along the three axes. The average symmetry of such domain network is, at least metrically, cubic although the symmetry of the domains themselves is orthorhombic. TEM studies showed that such structural arrangement is also apparent for $CaTi_{0.4}Fe_{0.6}O_{3-\delta}$. Different domains are connected via oxygen planes within an octahedral environment as corroborated by simulation of HRTEM images. These domains consist in irregular intergrowths of orthorhombic $CaTiO_3$- and $Ca_3TiFe_2O_8$-like phases along the b-axis. Mössbauer spectra are consistent with these results and show that the structure is sensitive to a fraction of Fe^{4+} as low as ca. 4% of the total amount of Fe. The high level of disorder within the microdomains, probably resulting from the short time (2 h) given to homogenize the material at high temperature, suggests that the excess of oxygen may be accommodated not only at the domain walls and the minority $CaTiO_3$-layers, but also in the border regions of the intergrown phases.

Acknowledgments

This work was supported by FCT (Portugal), Project PRAXIS P/CTM/14170/1998. J. Canales would like to thank the HiT Proton Project (EU-RTN) for funding, and a travel grant supported by the OSSEP Programme of the ESF. The authors would also like to thank SHEFC for supporting the TEM facilities at St Andrews.

References

[1] H. Iwahara, T. Esaka, T. Mangahara, J. Appl. Electrochem. 18 (1988) 173.
[2] D. Sutija, T. Norby, P.A. Osborg, P. Kofstad, in: S.C. Singhal, H. Iwahara (eds.), Proceedings of the Third International Symposium on Solid Oxide Fuel Cells, Electrochem. Soc. Proc. Vol. 93-4, Electrochemical Society, Pennington, NJ, 1993, p. 552.
[3] F.M. Figueiredo, J.C. Waerenborgh, V.V. Kharton, H. Näfe, J.R. Frade, Solid State Ionics 156 (2003) 371.
[4] T. Esaka, T. Fujii, K. Suwa, H. Iwahara, Solid State Ionics 40/41 (1990) 544.
[5] H. Itoh, H. Asano, K. Fukuroi, M. Nagata, H. Iwahara, J. Am. Ceram. Soc. 80 (6) (1997) 1359.
[6] F.M. Figueiredo, V.V. Kharton, J.C. Waerenborgh, A.P. Viskup, E.N. Naumovich, J.R. Frade, Influence of microstructure on the electrical properties of iron-substituted calcium titanate ceramics, J. Am. Ceram. Soc., in press.
[7] J.-C. Grenier, G. Schiffmacher, P. Caro, M. Pouchard, P. Hagenmuller, J. Solid State Chem. 20 (1977) 365.
[8] J.-C. Grenier, M. Pouchard, P. Hagenmuller, G. Schiffmacher, P. Caro, J. Phys. Colloq. C 7/38 (1977) 84.
[9] A.I. Becerro, C.A. McCammon, F. Langenhorst, R.J. Angel, F. Seifert, Phase Transit. 69 (1999) 133.
[10] C.A. McCammon, A.I. Becerro, F. Langenhorst, R.J. Angel, S. Marion, F. Seifert, J. Phys.: Condens. Matter 12 (2000) 2969.
[11] A.I. Becerro, F. Langenhorst, R. Angel, S. Marion, C. McCammon, F. Seifert, Phys. Chem. Chem. Phys. 2 (2000) 3933.

[12] J.C. Waerenborgh, F.M. Figueiredo, J.R. Frade, M.T. Colomer, J.R. Jurado, J. Phys.: Condens. Matter 13 (2001) 8171.
[13] M.A. Alario Franco, M.J.R. Henche, M. Vallet-Regí, J.M. González Calbet, J.C. Grenier, A. Wattiaux, P. Hagenmuller, J. Solid State Chem. 46 (1983) 23.
[14] M.A. Alario-Franco, J.M.G. Gonzalez-Calbet, M. Vallet-Regi, J.-C. Grenier, J. Solid State Chem. 49 (1983) 219.
[15] J.M. González Calbet, M. Vallet-Regí, M.A. Alario Franco, J.C. Grenier, Mater. Res. Bull. 18 (1983) 285.
[16] J.-C. Grenier, M. Pouchard, P. Hagenmuller, M.J.R. Henche, M. Vallet, J.M.G. Calbet, M.A. Alario-Franco, R. Chim. Minér. 20 (1983) 726.
[17] J.C. Waerenborgh, M.O. Figueiredo, J.M.P. Cabral, L.C.J. Pereira, J. Solid State Chem. 111 (1994) 300.
[18] JCPDS-ICDD file Number 42-423.
[19] J. Rodriguez-Carvajal, M. Vallet-Regí, J.M. González-Calbet, Mater. Res. Bull. 24 (1989) 423–430.
[20] A.A. Colville, Acta Crystallogr. B 26 (1970) 1469.
[21] S. Hovmöller, X. Zou, D. Neng Wang, J.M. Gonzalez-Calbet, M. Vallet-Regi, J. Solid State Chem. 77 (1988) 316.
[22] P.D. Battle, T.C. Gibb, S. Nixon, J. Solid State Chem. 79 (1989) 75.
[23] P.D. Battle, T.C. Gibb, P. Lightfoot, J. Solid State Chem. 84 (1990) 271.
[24] F.M. Figueiredo, M.R. Soares, V.V. Kharton, E.N. Naumovich, J.C. Waerenborgh, J.R. Frade, J. Electroceramics, in press.